NOTICE: This is the author’s version of a work that was accepted for publication in Advances in Space Research. Changes resulting from the publishing process, such as peer review, editing, corrections, structural formatting, and other quality control mechanisms may not be reflected in this document. Changes may have been made to this work since it was submitted for publication. A definitive version was subsequently published in Advances in Space Research, Vol. 52, Issue 12. (2013). doi: 10.1016/j.asr.2013.09.005

Improving the estimation of zenith dry tropospheric delays using regional surface meteorological data

X. Luo[a,*], B. Heck[a], J. L. Awange[a,b]

[a]Geodetic Institute, Karlsruhe Institute of Technology (KIT), Englerstraße 7, 76131 Karlsruhe, Germany

[b]Western Australian Centre for Geodesy and Institute for Geoscience Research, Curtin University, GPO Box U1987, WA 6845 Perth, Australia

---

Abstract

Global Navigation Satellite Systems (GNSS) are emerging as possible tools for remote sensing high-resolution atmospheric water vapour that improves weather forecasting through numerical weather prediction models. Nowadays, the GNSS-derived tropospheric zenith total delay (ZTD), comprising zenith dry delay (ZDD) and zenith wet delay (ZWD), is achievable with an accuracy of less than 1 cm. However, if no representative near-site meteorological information is available, the quality of the ZDD derived from tropospheric models is degraded, leading to inaccurate estimation of the water vapour component ZWD as difference between ZTD and ZDD. On the basis of freely accessible regional surface meteorological data, this paper proposes a height-dependent linear correction model for a priori ZDD. By applying the ordinary least-squares estimation (OLSE), bootstrapping (BOOT), and leave-one-out cross-validation (CROS) methods, the model parameters

*Corresponding author

Email addresses: xiaoguang.luo@kit.edu (X. Luo), bernhard.heck@kit.edu (B. Heck), J.Awange@curtin.edu.au (J. L. Awange)

are estimated and analysed with respect to outlier detection. The model validation is carried out using GNSS stations with near-site meteorological measurements. The results verify the efficiency of the proposed ZDD correction model, showing a significant reduction in the mean bias from several centimetres to about 5 mm. The OLSE method enables a fast computation, while the CROS procedure allows for outlier detection. All the three methods produce consistent results after outlier elimination, which improves the regression quality by about 20% and the model accuracy by up to 30%.

Keywords: GNSS meteorology; Zenith tropospheric delays; Regional surface meteorological data; Outlier detection; Linear regression

1. Introduction

For nearly 20 years, Global Navigation Satellite Systems (GNSS), such as the U.S. Global Positioning System (GPS), have been used to remote sense atmospheric water vapour based on the delays of GNSS signals when propagating through the Earth's troposphere (Bevis et al., 1992; Rocken et al., 1993). At sea level, the tropospheric delay in metric units is approximately 2.3 m in the zenithal direction (Hofmann-Wellenhof et al., 2008, p. 135), and it increases to more than 10 m for an elevation angle of 10°. According to Hopfield (1969), the tropospheric delay can be subdivided into a predominant and well-behaved dry part and a complementary and volatile wet part. The dry delay term amounts to about 90% of the total delay and can be accurately determined using air density (Davis et al., 1985). Under the assumption of hydrostatic equilibrium, the air density is obtainable from ground pressure measurements. In contrast to the dry part, it is very difficult to evaluate the wet delay term due to the high temporal and spatial variability of atmospheric water vapour (Bevis et al., 1992).

Nowadays, the zenith total delay (ZTD) can be obtained with an accuracy of less than 1 cm from GNSS data analysis (Douša, 2004; Byun and Bar-Sever, 2009; Chen et al., 2011). In addition, various studies have shown that the quality of the GNSS-derived ZTD can be considerably improved by specifying an appropriate stochastic model characterising the precision and correlations of GNSS measurements (Jin and Park, 2005; Luo et al., 2008; Jin et al., 2010). If representative meteorological data, either observed near GNSS sites or derived from numerical weather models, are available, the zenith dry delay (ZDD) can be accurately computed by means of tropospheric models, e.g., the Saastamoinen model (Saastamoinen, 1973). The complementary zenith wet delay (ZWD) is then determined as the difference between ZTD and ZDD (Jin and Luo, 2009):

$$\mathrm{ZWD} = \mathrm{ZTD} - \mathrm{ZDD}, \tag{1}$$

which can be converted into the so-called precipitable water (PW) in metric units using $\mathrm{PW} \approx 0.15 \times \mathrm{ZWD}$ (Bevis et al., 1994). Past studies have demonstrated that the PW derived from GNSS can reach an accuracy of about 2 mm (Boccolari et al., 2002). High-quality tropospheric delay and PW estimates provide valuable information for weather forecasting (Awange, 2012, Sect. 10.4.1). For example, Poli et al. (2007, 2008) reported that the assimilation of GNSS-derived ZTD into numerical weather prediction models leads to improved forecasts of temperature, wind, and precipitation. Sasse (2011) showed that a combination of GPS and COSMO (Consortium for Small-scale

Modeling) data enhances the simulated regional precipitation in about 50% of the considered cases. Furthermore, a unique opportunity for GNSS-based water vapour determination is created by the establishment of networks of continuously operating reference stations (CORS), such as the NOAA GPS-IPW network in the USA (Wolfe and Gutman, 2000), the GEONET in Japan (Iwabuchi et al., 2000), the AGNES in Switzerland (Troller et al., 2006b), and the SAPOS® in Germany (Gendt et al., 2004). By applying GNSS tomography in dense networks of CORS, three-dimensional water vapour fields can be reconstructed at high temporal and spatial resolution (Troller et al., 2006a; de Haan and van der Marel, 2008; Bender et al., 2011a). As Bender et al. (2011b) showed, a combination of GPS, GLONASS, and Galileo observations can increase the resolution of the recovered humidity fields up to 30 km horizontally, 300 m vertically, and 15 min temporally.

The ZTD in Eq. (1) can be precisely estimated depending on satellite geometry, quality of the mapping function, and data availability (e.g., elevation mask). Therefore, the key issue for an accurate ZWD evaluation is the quality of the ZDD, which will be strongly degraded if no representative near-site meteorological data are available. In this case, site-specific meteorological parameters, such as pressure (p), temperature (T), and relative humidity (rh), are usually obtained by extrapolating the standard atmosphere (e.g., NOAA/NASA/USAF, 1976) from mean sea level (MSL) to GNSS station level (H_S). The ZDD computed based on the extrapolated meteorological data is called a priori ZDD, which is temporally invariable and cannot be used directly to derive the ZWD. For a reliable ZDD determination, meteorological input is indispensable. This can be gained from regional meteorological sites on which both surface measurements (MET_M) and station altitudes (H_M) above MSL are available. To derive representative p and T values for GNSS sites, Bai and Feng (2003) suggested a two-step procedure: first, deducing the MSL values from MET_M (i.e., $H_M \rightarrow$ MSL), and second, deducing the station level data for GNSS sites from the MSL values (i.e., MSL $\rightarrow H_S$). Based on the difference between H_S and H_M, Karabatić et al. (2011) extrapolated the pressure and temperature data from the nearest meteorological station to the GNSS site of interest.

Differing from the two approaches mentioned above, where the meteorological parameters p, T, and rh are considered, this paper uses freely accessible regional surface meteorological data to derive a height-dependent correction model for the a priori ZDD. The rest of this paper is organised as follows. Sect. 2 describes the study area and the data used. In Sect. 3, the ZDD correction model is presented, along with different methods for parameter estimation. The results are discussed in Sect. 4, including quality assessments and model validation. Finally, Sect. 5 provides concluding remarks and an outlook on future research work.

2. Study Area and Data

The study area is located in southwest Germany and is well covered by the GNSS Upper Rhine Graben Network (GURN), which was established to, among other things, automatically determine regional atmospheric water vapour at high temporal and spatial resolution (Fuhrmann et al., 2010; Mayer et al., 2012). This area is the warmest region of Germany, with hot summer and mild winter. Such meteorological conditions are due to frequent southwest air mass flows from the western Mediterranean. The amount of precipitation increases towards the south and reaches the maximum in the southeast and the Black Forest region.

As Fig. 1 shows, a total of 21 stations of the German Meteorological Service (DWD) are used, which are homogeneously distributed in the investigation area, with altitudes ranging from 37 to 977 m above MSL. The freely accessible surface metrological data can be downloaded from the DWD web site[1] and have a temporal resolution of 6 h. The period of investigation is DOY2008:276–285, corresponding to October 2–11, 2008 (Fuhrmann et al., 2010). Apart from the DWD sites, four GNSS stations (dill, efbg, muej, bfo1) from the Integrated German Geodetic Reference Network (GREF) are also included, which are symbolised by filled triangles in Fig. 1. Considering that surface metrological measurements (MET_R) are available on these GNSS sites, they are used to assess the accuracy of the proposed ZDD correction model. The altitudes of the GREF stations are representative and vary between 181 and 647 m above MSL. Additional information about the DWD and GREF meteorological data is provided in Tables 1 and 2, respectively.

FIGURE 1

Table 1: Resolution of the DWD surface meteorological data.

Parameter	**Notation**	**Resolution**
Air pressure	p_M	0.1 hpa
Temperature	T_M	0.1°C
Relative humidity	rh_M	1%
Time interval	Δt_M	6 h

[1] www.dwd.de / Services A-Z / Freely Available Climate Data

Table 2: Resolution of the GREF surface meteorological data and the site altitudes above mean sea level (MSL).

GREF site	**Altitude** H_S [m]	**Time interval**[1] Δt_R [s]	**Resolution**[1] MET_R
dill	181	10	R: RINEX
efbg	355	900	p_R: 0.1 hpa
muej	548	10	T_R : 0.1°C
bfo1	647	15	rh_R: 0.1%

[1] From RINEX meteorological data files

3. Methodology

To achieve a better understanding of the height-dependent ZDD correction model, its principle is schematically illustrated in Fig. 2. For an arbitrary GNSS site with altitude H_S above MSL, the site-specific pressure p_S [hPa], temperature T_S [K], and relative humidity rh_S [%] can be obtained by extrapolating the standard atmosphere with p_0, T_0, and rh_0 at MSL(Berg, 1948, pp. 122, 135; Dach et al., 2007, p. 243). According to Troller (2004, p. 16), it is possible to calculate the ZDD as

$$ZDD = 0.002277D(p - 0.155471e), \tag{2}$$

where D considers the variation of gravity in the tropospheric air column above the site. It can be computed based on a normal gravity field as

$$D = 1 + 0.0026\cos(2\varphi) + 0.00028H, \tag{3}$$

where φ is the site latitude and H [km] is the site height above MSL. Depending on T [K] and rh [%], the partial pressure of water vapour e [hPa] in Eq. (2) is obtained by means of the formula

$$e = \left(\frac{rh}{100}\right) \exp\left(-37.2465 + 0.2131665T - 0.000256908T^2\right), \qquad (4)$$

where exp(·) is the exponential function (Xu, 2003, p. 52). Substituting (p_S, T_S, rh_S) and H_S into Eqs. (2)–(4), which are also provided by Mayer (2006, pp. 115, 140, 141), the resulting a priori ZDD of GNSS signals is temporally invariable and is denoted as $ZDD(H_S)$.

FIGURE 2

Using surface measurements from regional meteorological sites located at representative heights (p_M, T_M, rh_M), one can directly obtain the ZDD, which is termed as $ZDD(MET_M)$ and predominantly reflects pressure variations (see Eq. (2)). On the other hand, based on the standard atmosphere and the altitudes of the meteorological stations H_M above MSL, the a priori $ZDD(H_M)$ can be derived, which is also invariable over time. The discrepancy between $ZDD(MET_M)$ and $ZDD(H_M)$ is utilised to establish a linear height-dependent ZDD correction model, i.e.,

$$\Delta ZDD_M = ZDD(MET_M) - ZDD(H_M) = aH_M + b = f(H_M), \qquad (5)$$

where a (slope) and b (intercept) are the unknown regression coefficients that must be reliably estimated. Assuming that, on a regional scale of hundreds of kilometres, the function $f(\cdot)$ is also valid for the GNSS sites which are located in the same area, the correction value for the a priori $ZDD(H_S)$ is

$$\Delta ZDD_S = f(H_S) = aH_S + b. \qquad (6)$$

Accordingly, the corrected ZDD can be expressed as

$$ZDD_S = ZDD(H_S) + \Delta ZDD_S, \tag{7}$$

which is supposed to vary temporally and is more suitable than the a priori $ZDD(H_S)$ for determining the ZWD from Eq. (1).

In this paper, the regression coefficients a and b of Eq. (5) are estimated using three different methods, namely ordinary least-squares estimation (OLSE), bootstrapping (BOOT), and leave-one-out cross-validation (CROS) in order to find a computationally efficient and statistically reliable approach, particularly in the presence of outliers. The OLSE method minimises the squared sum of residuals v_i, i.e.,

$$\sum_{i=1}^{n} v_i^2 = \sum_{i=1}^{n} [(ax_i + b) - y_i]^2 \rightarrow \min, \tag{8}$$

where n is the number of the used meteorological sites, x_i and y_i are the values of H_M and ΔZDD_M, respectively (see Eq. (5)). For a reliable estimation of the regression coefficients, outlier detection is performed by analysing the so-called studentised residuals r_i defined as

$$r_i = \frac{v_i}{\hat{\sigma}_{v_i}} = \frac{v_i}{\hat{\sigma}_0 \sqrt{\boldsymbol{Q}_{vv}(i,i)}} \sim \tau_f, \tag{9}$$

where $\hat{\sigma}_0^2$ is the a posteriori variance factor, and $\boldsymbol{Q}_{vv}(i,i)$ is the i-th diagonal element of the residual cofactor matrix $\boldsymbol{Q}_{vv}$ (Cook and Weisberg, 1982, p. 18). The studentised residual follows Pope's τ-distribution with f degrees of freedom (f: redundancy of the OLSE; Pope, 1976, p. 15; Heck, 1981b), which can be related to Student's t-distribution with $f-1$ degrees of freedom for f ? (Beckman and Trussell, 1974; Heck, 1981a):

$$t_i = \sqrt{\frac{(f-1)r_i^2}{f - r_i^2}} \sim t_{f-1}. \tag{10}$$

The outliers are detected at a significance level of α if $t_i > t_{f-1;1-\alpha/2}$, where $t_{f-1;q}$ is the q-quantile of Student's t-distribution with $f-1$ degrees of freedom, and α denotes the probability of committing a Type I error. Note that the identified outliers can be attributed to both improper meteorological measurements and site-specific environments, resulting in considerable deviations from the assumed linear regression model.

The bootstrapping (BOOT) method chooses random samples from the n pairs of (H_M, $6ZDD_M$) with replacement, meaning that a particular data point could appear multiple times in a bootstrap sample. The number of elements in each bootstrap sample is equal to the number of elements in the original data set (i.e., n). The OLSE method is then applied to each bootstrap sample, and the final estimates of the regression coefficients are the arithmetic means of all individual solutions. Since the statistics of the subsamples provide better information about the characteristics of the population than the statistics computed from the full data set, the BOOT algorithm produces more reliable parameter estimates and allows assessing the statistical significance of results. A major disadvantage of this method, however, is the high computational cost caused by the resampling procedure. For a more detailed discussion of bootstrapping, the reader is referred to Efron (1982, Chap. 5) and Trauth (2007, pp. 66, 74).

The leave-one-out cross-validation (CROS) method is also employed to evaluate the goodness-of-fit of the regression (Trauth, 2007, p. 77). It works by first temporarily removing the i-th element (x_i, y_i), and then using the remaining $n-1$ observations to estimate the regression line with the OLSE method. Afterwards, the i-th data point is predicted from the resulting regression model, meaning that $f_i(x_i) = a_i x_i + b_i$. The difference between the observation y_i and the prediction $f_i(x_i)$, i.e.,

$$\hat{r}_i = y_i - f_i(x_i), \tag{11}$$

is known as prediction error, which in the optimal case follows a normal distribution with zero mean. Relying upon the prediction sum of squares provided by Allen (1974), the mean prediction error over all n data points can be written as

$$\hat{r} = \left[\frac{1}{n} \sum_{i=1}^{n} (\underbrace{y_i - f_i(x_i)}_{z_i})^2 \right]^{\frac{1}{2}} . \tag{12}$$

The CROS method provides not only valuable information about the goodness- of-fit of the regression, but also the possibility of detecting outliers through analysing the prediction error. This technique can also be used for quality control in other fields, e.g., spatial and temporal prediction.

4. Discussion of the results

Since the efficiency of the above-discussed methods in estimating regression coefficients can be considerably affected by outliers, Fig. 3 first illustrates a representative example of outlier detection and its impact on the results of linear regression. For the time interval 6–12 h UTC on DOY2008:277 (i.e., October 3, 2008), Fig. 3a depicts that the outlier, DWD site Kahler Asten, can be clearly identified at a significance level of ↲ = 5% based on studentised residuals and t-statistics, given by Eqs. (9) and (10), respectively. Fig. 3b compares the resulting regression lines determined by means of the OLSE method, where the outlier elimination leads to a significant change in the slope estimate from -0.27 to 0.23 [cm/km]. Moreover, after removing the outlier, the width of the 95% prediction bounds is reduced, indicating higher reliability in forecasting a future data point. This particular DWD station is considered as outlier in about 80% of all regressions, which is due to the mountainous location (see Fig. 1) and the humid climate rather than improper meteorological measurements. For the entire period of investigation, Fig. 3c shows that, in most cases, the outlier removal increases the absolute values of the bootstrap estimates of Pearson's correlation coefficients between H_M and $6ZDD_M$. This implies a stronger linear trend in the outlier-free bivariate data set and verifies the validity of the linear correction model given by Eq. (5). Fig. 3d displays the mean prediction errors produced by the cross-validation method (see Eq. (12)), emphasising once again the necessity of statistically rigorous outlier detection.

FIGURE 3

For the same example as shown in Fig. 3b, Fig. 4 displays the histograms of the slope (see a and b) and intercept (see c and d) estimates obtained from bootstrapping with 5000 samples. If outliers are preliminarily removed (see b and d), the determined regression coefficients illustrate smaller scatters, indicating more precise parameter estimates. Comparing Fig. 4a and b with each other, the significant change in the mean slope from -0.25 to

0.27 [cm/km] coincides with the results presented in Fig. 3b.

FIGURE 4

Fig. 5 provides an example of linear regression using the cross-validation method, which enables outlier detection through analysing the prediction errors $r5_i$ defined by Eq. (11). Examining the absolute values of $r5_i$ shown in Fig. 5a, the outlier is clearly visible, corresponding to the results displayed in Fig. 3a. Under the assumption of a normal distribution with zero mean, the statistical significance of $r5_i$ can be evaluated (Trauth, 2007, p. 78). To demonstrate the influence of outlier elimination, Fig. 5b depicts the estimated regression lines. It can be seen that the correct result is only obtained in the case where the outlier is left out as the i-th element (cf. Fig. 3b). Like the bootstrapping method, the mean solution from cross-validation is also strongly biased in the presence of outliers (cf. Fig. 4a and c).

FIGURE 5

After removing the detected outliers, the final ZDD correction model is estimated by means of the ordinary least-squares estimation (OLSE), bootstrapping (BOOT), and cross-validation (CROS) methods. The resulting linear regression coefficients are compared in Fig. 6. For both the slope and intercept parameters, the outcomes are largely consistent, where slight differences in the slope estimates are visible on DOY2008:279 (i.e., October 5, 2008). This is due to the significant increase in the amount of precipitation on this particular day, as shown in Fig. 7b. The results from the OLSE method are almost identical to those from the BOOT and CROS approaches, which are in fact advanced in view of statistical reliability. This suggests the appropriateness of the OLSE technique in determining the ZDD correction model based on outlier-free data sets. The main advantage of the OLSE method compared to the other two alternatives is its fast computation.

FIGURE 6

To assess the goodness-of-fit of the linear regression, the model error is defined as the standard deviation of the least-squares residuals v_i provided by Eq. (8). As an alternative, the mean prediction error *r5* resulting from the cross-validation process can be used for quality assessments (see Eq. (12)). As Fig. 7a illustrates, the model error is less than 5 mm in most cases. Moreover, the outlier removal considerably reduces the mean model error by about 20%, from 0.43 to 0.33 cm. By comparing the model error with the sum of precipitation recorded on all DWD sites contributing to the linear regression (see Fig. 7b), one can clearly discern that the regression quality decreases with increasing air humidity. In other words, it is more difficult to reliably derive the ZDD from Eq. (2) under humid atmospheric conditions.

FIGURE 7

Using the GREF stations with near-site meteorological measurements (MET_R; see Table 2), the accuracy of the proposed ZDD correction model can be evaluated by comparing $ZDD(MET_R)$ with the corrected a priori ZDD obtained from Eq. (7). The correction term 6ZDD_S is computed with and without outliers by means of Eq. (6), and the resulting corrected values are denoted as ZDD_S^O (with outliers) and ZDD_S (without outliers), respectively. Taking the GREF sites with the minimum (dill) and the maximum altitude (bf01) for example, Fig. 8 displays the ZDD (see a and c) as well as the bias with respect to $ZDD(MET_R)$ (see b and d). The black dashed lines shown in Fig. 8a and c represent the temporally invariable a priori $ZDD(H_S)$. After adding the correction term δZDD_S to $ZDD(H_S)$, the temporal variations in $ZDD(MET_R)$ can be largely reconstructed in spite of the low temporal and spatial resolution of the freely accessible DWD surface meteorological data (see Fig. 1 and Table 1). Comparing Fig. 8a and c, the positive impact of outlier removal appears to be more obvious for the site bf01. This can be explained by its higher altitude (dill: 181 m, bf01: 647 m), making this site suffer more strongly from the identified outlier (see, e.g., Fig. 3b). Considering $ZDD(MET_R)$ as the reference, the biases of the a priori ZDD depicted in Fig. 8b and d reach up to about 5 cm, and are reduced to predominantly less than 1 cm by means of the ZDD correction model, showing a significant bias reduction of up to 80%.

FIGURE 8

Relying upon the difference between $ZDD(MET_R)$ and ZDD_S, the model accuracy is assessed by computing the mean absolute bias (MAB) defined as

$$MAB = \frac{1}{N} \sum_{j=1}^{N} |ZDD(MET_{R,j}) - ZDD_{S,j}| , \qquad (13)$$

where N is the number of differences and depends on the sampling interval of the GREF meteorological data (see Table 2). Table 3 presents the MAB values for all GREF stations, where the correction terms are derived with (ΔZDD^{O}_{S}) and without outliers (ΔZDD_{S}). In the absence of outliers, a model accuracy of about 5 mm can be achieved. For high-altitude sites, such as muej and bfo1, the outlier elimination seems to be particularly beneficial, which has also been observed in Fig. 8. In this case, the model accuracy can be improved by up to about 30% if outliers are removed prior to estimating the final regression coefficients.

Table 3: Accuracy assessment of the ZDD correction model using representative GREF stations with near-site meteorological data (see Table 2).

GREF site	dill	efbg	muej	bfo1
Site altitude H_S [m]	181	355	548	647
MAB(with outlier) [mm]	4.5	8.2	6.6	6.2
MAB(without outlier) [mm]	**4.6**	7.8	**5.2**	**4.5**
Improvement [%]	-2	5	**21**	**27**

In order to verify the adequacy of the linear ZDD correction model, the second-degree polynomial regression is performed using

$$\Delta ZDD_M = aH_M^2 + bH_M + c = f(H_M), \tag{14}$$

where H_M denotes the altitudes of the regional meteorological sites above MSL (cf. Eq. (5)). After eliminating outliers, the final regression coefficients a, b, c are also determined by means of the OLSE, BOOT, and CROS methods, producing largely consistent parameter estimates. Taking the results from the OLSE as an example, Fig. 9 compares the model error and the corrected ZDD with respect to the order of regression. As can be seen in Fig. 9a, only insignificant enhancements in the regression quality are achieved by applying a quadratic polynomial. In Fig. 9b, the corrected ZDD using the linear and quadratic models are almost identical, indicating the adequacy of the proposed linear approach. For all GREF sites, Table 4 presents the model accuracy with regard to the degree of regression (see Eq. (13)). The improvements in the MAB values caused by the quadratic regression are marginal, where Fig. 9b actually represents the best case scenario.

FIGURE 9

Table 4: Model accuracy [mm] of the ZDD correction using different orders of regression (see Eq. (13), without outliers, OLSE method).

Regression model	dill (181 m)	efbg (355 m)	muej (548 m)	bfo1 (647 m)
Linear	4.6	7.8	5.2	4.5
Quadratic	4.8	7.8	4.9	4.4
Improvement [%]	-4	0	**6**	2

5. Conclusions and Outlook

This paper proposed a practicable approach for a reliable and accurate determination of zenith dry tropospheric delays of GNSS signals if there are no representative near-site meteorological data available. The main findings of this contribution can be summarised as follows:

1. Using freely accessible surface data from regional meteorological sites, a height-dependent linear regression model is developed to correct the a priori zenith dry delay (ZDD) derived based on the standard atmosphere. Following a residual-based outlier detection, the final regression coefficients are estimated by means of the ordinary least-squares estimation (OLSE), bootstrapping (BOOT), and cross-validation (CROS)

methods, which produce largely consistent results. While the OLSE approach enables a fast computation, the CROS method allows outlier detection through analysing the prediction error.

2. In order to assess the performance of the proposed ZDD correction model, model error evaluates the goodness-of-fit of linear regression, while model accuracy examines the overall deviation from ground truth. Within the framework of the presented case study, the model error (accuracy) is below (near) 5 mm in most cases. Furthermore, the statistically rigorous outlier removal significantly reduces the model error by about 20%, and improves the model accuracy by up to 30%.
3. If outliers are appropriately eliminated before estimating the final regression coefficients, the use of a quadratic polynomial only insignificantly enhances the results of ZDD correction, indicating the adequacy of the proposed linear approach.

Future research will focus on the refinement, verification, and application of the proposed ZDD correction model. For example, apart from altitude information, locations of regional meteorological sites should be taken into account when computing the correction values. Considering the availability of some meteorological information with short time latency, the possibility of applying the suggested method in near real time will be studied based on a larger number of meteorological and GNSS stations. Moreover, a comparison with other approaches, e.g., proposed by Bai and Feng (2003) and Karabatić et al. (2011), is also planned, where additional data sets should be included. Finally, the refined ZDD correction model will be applied to regional water vapour determination using GNSS alone (Fuhrmann et al., 2010), or in combination with other sensors such as Interferometric Synthetic Aperture Radar (InSAR; Alshawaf et al., 2012).

Acknowledgements

X. Luo gratefully acknowledges the German Research Foundation (DFG) and the Geodetic Institute of the Karlsruhe Institute of Technology (KIT) for supporting this research work. J. L. Awange appreciates the financial support from the Alexander von Humboldt Foundation (Ludwig Leichhardt's Memorial Fellowship) and the Curtin Research Fellowship. He is grateful to his host Prof. B. Heck for the enjoyable working atmosphere at the Geodetic Institute, KIT. Two anonymous reviewers are deeply acknowledged for their valuable comments. This is The Institute for Geoscience Research (TIGeR) publication No. 476.

References

Allen, D. M. (1974). The relationship between variable selection and data augmentation and a method for prediction. *Technometrics*, 16(1):125–127. doi:10.1080/00401706.1974.10489157.

Alshawaf, F., Fuhrmann, T., Heck, B., Hinz, S., Knöpfler, A., Luo, X., Mayer, M., Schenk, A., Thiele, A., and Westerhaus, M. (2012). Integration of InSAR and GNSS observations for the determination of atmospheric water vapour. In: J. M. Krisp et al. (eds.), *Earth Observation of Global Changes (EOGC)*, Proceedings of EOGC2011, Munich, Germany, April 13–15, Lecture Notes in Geoinformation and Cartography, Springer-Verlag, Berlin Heidelberg, pp. 147–162. doi:10.1007/978-3-642-32714-8_10.

Amante, C. and Eakins, B. W. (2009). ETOPO1 1 arc-minute global relief model: Procedures, data sources and analysis. NOAA Technical Memorandum NESDIS NGDC-24, National Geophysical Data Center, Marine Geology and Geophysics Division, Boulder, CO, USA.

Awange, J. L. (2012). *Environmental Monitoring Using GNSS: Global Navigation Satellite Systems*. Springer-Verlag, Berlin Heidelberg.

Bai, Z. and Feng, Y. (2003). GPS water vapor estimation using interpolated surface meteorological data from Australian Automatic Weather Stations. *J. Glob. Position. Syst.*, 2(2):83–89.

Beckman, R. J. and Trussell, H. J. (1974). The distribution of an arbitrary studentized residual and the e↵ects of updating in multiple regression. *J. Amer. Stat. Assoc.*, 69(345):199–201. doi:10.2307/2285524.

Bender, M., Dick, G., Ge, M., Deng, Z., Wickert, J., Kahle, H.-G., Raabe, A., and Tetzla↵, G. (2011a). Development of a GNSS water vapour tomography system using algebraic reconstruction techniques. *Adv. Space Res.*, 47(10):1704–1720. doi:10.1016/j.asr.2010.05.034.

Bender, M., Stosius, R., Zus, F., Dick, G., Wickert, J., and Raabe, A. (2011b). GNSS water vapour tomography – Expected improvements by combining GPS, GLONASS and Galileo observations. *Adv. Space Res.*, 47(5):886–897. doi:10.1016/j.asr.2010.09.011.

Berg, H. (1948). *Allgemeine Meteorologie: Einführung in die Physik der Atmosphäre*. Dümmler Verlag, Bonn.

Bevis, M., Businger, S., Chiswell, S., Herring, T. A., Anthes, R. A., Rocken, C., and Ware, R. H. (1994). GPS meteorology: Mapping zenith wet delays onto precipitable water. *J. Appl. Meteorol. Clim.*, 33(3):379–386. doi:10.1175/1520-0450(1994)033<0379:GMMZWD>2.0.CO;2.

Bevis, M., Businger, S., Herring, T. A., Rocken, C., Anthes, R. A., and Ware, R. H. (1992). GPS meteorology: Remote sensing of atmospheric water vapor using the global positioning system. *J. Geophys. Res.*, 97(D14):15787–15801. doi:10.1029/92JD01517.

Boccolari, M., Fazlagić, S., Frontero, P., Lombroso, L., Pugnaghi, S., Santangelo, R., Corradini, S., and Teggi, S. (2002). GPS zenith total delays and precipitable water in comparison with special meteorological observations in Verona (Italy) during MAP-SOP. *Ann. Geophys.*, 45(5):599–608. doi:10.4401/ag-3534.

Byun, S. H. and Bar-Sever, Y. E. (2009). A new type of troposphere zenith path delay product of the international GNSS service. *J. Geod.*, 83(3–4):367–373. doi:10.1007/s00190-008-0288-8.

Chen, Q., Song, S., Heise, S., Liou, Y.-A., Zhu, W., and Zhao, J. (2011). Assessment of ZTD derived from ECMWF/NCEP data with GPS ZTD over China. *GPS Solut.*, 15(4):415–425. doi:10.1007/s10291-010-0200-x.

Cook, R. D. and Weisberg, S. (1982). *Residuals and Influence in Regression.* Chapman & Hall, New York.

Dach, R., Hugentobler, U., Fridez, P., and Meindl, M. (2007). Bernese GPS

Software Version 5.0. Astronomical Institute, University of Bern, Bern, Switzerland.

Davis, J. L., Herring, T. A., Shapiro, I. I., Rogers, A. E. E., and Elgered, G. (1985). Geodesy by radio interferometry: E↵ects of atmospheric modeling errors on estimates of baseline length. *Radio Sci.*, 20(6):1593–1607. doi:10.1029/RS020i006p01593.

de Haan, S. and van der Marel, H. (2008). Observing three dimensional water vapour using a surface network of GPS receivers. *Atmos. Chem. Phys. Discuss.*, 8(5):17193–17235. doi:10.5194/acpd-8-17193-2008.

Douša, J. (2004). Evaluation of tropospheric parameters estimated in various routine GPS analysis. *Phys. Chem. Earth*, 29(2–3):167–175. doi:10.1016/j.pce.2004.01.011.

Efron, B. (1982). *The Jackknife, the Bootstrap and Other Resampling Plans*. CBMS-NSF Regional Conference Series in Applied Mathematics, No. 38, Society for Industrial and Applied Mathematics, Philadelphia.

Fuhrmann, T., Knöpfler, A., Mayer, M., Luo, X., and Heck, B. (2010). Zur GNSS-basierten Bestimmung des atmosphärischen Wasserdampfgehalts mittels Precise Point Positioning. Schriftenreihe des Studiengangs Geodäsie und Geoinformatik, Band 2/2010, Karlsruhe Institute of Technology (KIT), KIT Scientific Publishing, Karlsruhe, Germany.

Gendt, G., Dick, G., Reigber, C., Tomassini, M., Liu, Y. Z., and Ramatschi, M. (2004). Near real time GPS water vapor monitoring for numerical weather prediction in Germany. *J. Meteorol. Soc. Jpn.*, 82(1B):361–370.

Heck, B. (1981a). Der Einfluß einzelner Beobachtungen auf das Ergebnis einer Ausgleichung und die Suche nach Ausreißern in den Beobachtungen. *Allgemeine Vermessungs-Nachrichten (AVN)*, 88(1):17–34.

Heck, B. (1981b). Statistische Ausreißerkriterien zur Kontrolle geodätischer Beobachtungen. In: R. Conzett et al. (eds.), *Ingenieurvermessung '80*, Beiträge zum VIII. Internationalen Kurs für Ingenieurvermessung, Zurich, Switzerland, September 24–October 1, 1980, Dümmler, Bonn, B10/1–12.

Hofmann-Wellenhof, B., Lichtenegger, H., and Wasle, E. (2008). *GNSS-Global Navigation Satellite Systems: GPS, GLONASS, Galileo & more*. Springer-Verlag, Wien.

Hopfield, H. S. (1969). Two-quartic tropospheric refractivity profile for correcting satellite data. *J. Geophys. Res.*, 74(18):4487–4499. doi:10.1029/JC074i018p04487.

Iwabuchi, T., Naito, I., and Mannoji, N. (2000). A comparison of Global Positioning System retrieved precipitable water vapor with the numerical weather prediction analysis data over the Japanese Islands. *J. Geophys. Res.*, 105(D4):4573–4585. doi:10.1029/1999JD901007.

Jin, S. and Luo, O. (2009). Variability and climatology of PWV from global 13-year GPS observations. *IEEE Trans. Geosci. Remote*, 47(7):1918–1924. doi:10.1109/TGRS.2008.2010401.

Jin, S. G., Luo, O., and Ren, C. (2010). E↵ects of physical correlations on long-distance GPS positioning and zenith tropospheric delay estimates. *Adv. Space Res.*, 46(2):190–195. doi:10.1016/j.asr.2010.01.017.

Jin, S. G. and Park, P. H. (2005). A new precision improvement in zenith tropospheric delay estimation by GPS. *Curr. Sci.*, 89(6):997–1000.

Karabatić, A., Weber, R., and Haiden, T. (2011). Near real-time estimation of tropospheric water vapour content from ground based GNSS data and its potential contribution to weather now-casting in Austria. *Adv. Space Res.*, 47(10):1691–1703. doi:10.1016/j.asr.2010.10.028.

Luo, X., Mayer, M., and Heck, B. (2008). Improving the stochastic model of GNSS observations by means of SNR-based weighting. In: M. G. Sideris (ed.), *Observing our Changing Earth*, Proceedings of the 2007 IAG General Assembly, Perugia, Italy, July 2–13, IAG Symposia, Vol. 133, Springer-Verlag, Berlin Heidelberg, pp. 725–734. doi:10.1007/978-3-540-85426-5_83.

Mayer, M. (2006). Modellbildung für die Auswertung von GPS-Messungen im Bereich der Antarktischen Halbinsel. Deutsche Geodätische Kommission, C597, Verlag der Bayerischen Akademie der Wissenschaften, München.

Mayer, M., Knöpfler, A., Heck, B., Masson, F., Ulrich, P., and Ferhat, G. (2012). GURN (GNSS Upper Rhine Graben Network): Research goals and first results of a transnational geo-scientific network. In: S. C. Kenyon et al. (eds.), *Geodesy for Planet Earth*, Proceedings of the 2009 IAG Symposium, Buenos Aires, Argentina, August 31–September 4, IAG Symposia, Vol. 136, Springer-Verlag, Berlin Heidelberg, pp. 673–681. doi:10.1007/978-3-642-20338-1_83.

NOAA/NASA/USAF (1976). U.S. Standard Atmosphere, 1976. NOAA–S/T 76–1562, U.S. Government Printing Office, Washington, D.C., USA.

Poli, P., Moll, P., Rabier, F., Desroziers, G., Chapnik, B., Berre, L., Healy, S. B., Andersson, E., and El Guelai, F.-Z. (2007). Forecast impact studies of zenith total delay data from European near real-time GPS stations in Météo France 4DVAR. *J. Geophys. Res.*, 112, D06114. doi:10.1029/2006JD007430.

Poli, P., Pailleux, J., Ducrocq, V., Moll, P., Rabier, F., Mauprivez, M., Dufour, S., Grondin, M., Carvalho, F., Issler, J.-L., De Latour, A., and Ries, L. (2008). Weather report: Meteorological applications of GNSS from space and on the ground. *Inside GNSS*, 3(8):30–39.

Pope, A. J. (1976). The statistics of residuals and the detection of outliers. NOAA Technical Report NOS 65 NGS 1, Rockville, MD, USA.

Rocken, C., Ware, R., Van Hove, T., Solheim, F., Alber, C., Johnson, J., Bevis, M., and Businger, S. (1993). Sensing atmospheric water vapor with the global positioning system. *Geophys. Res. Lett.*, 20(23):2631–2634. doi:10.1029/93GL02935.

Saastamoinen, J. (1973). Contribution to the theory of atmospheric refraction: Part II. Refraction corrections in satellite geodesy. *Bull. Geod.*, 107(1):13–34. doi:10.1007/BF02522083.

Sasse, R. (2011). *Analyse des regionalen atmosphärischen Wasserhaushalts unter Verwendung von COSMO-Simulationen und GPS-Beobachtungen*. PhD thesis, Department of Civil Engineering, Geo and Environmental Sciences, Karlsruhe Institute of Technology (KIT), Karlsruhe, Germany.

Trauth, M. H. (2007). *MATLAB® Recipes for Earth Sciences*. Springer-Verlag, Berlin Heidelberg, 2^{nd} edition.

Troller, M. (2004). GPS based determination of the integrated and spatially distributed water vapor in the troposphere. Geodätisch-geophysikalische Arbeiten in der Schweiz, Schweizerische Geodätische Kommission, Vol. 67, Zürich.

Troller, M., Geiger, A., Brockmann, E., Bettems, J.-M., Bürki, B., and Kahle, H.-G. (2006a). Tomographic determination of the spatial distribution of water vapor using GPS observations. *Adv. Space Res.*, 37(12):2211–2217. doi:10.1016/j.asr.2005.07.002.

Troller, M., Geiger, A., Brockmann, E., and Kahle, H.-G. (2006b). Determination of the spatial and temporal variation of tropospheric water vapour using CGPS networks. *Geophys. J. Int.*, 167(2):509–520. doi:10.1111/j.1365-246X.2006.03101.x.

Wolfe, D. E. and Gutman, S. I. (2000). Developing an operational, surface-based, GPS, water vapor observing system for NOAA: Network design and results. *J. Atmos. Ocean. Tech.*, 17(4):426–440. doi:10.1175/1520-0426(2000)017<0426:DAOSBG>2.0.CO;2.

Xu, G. (2003). *GPS: Theory, Algorithms and Applications*. Springer-Verlag, Berlin Heidelberg.

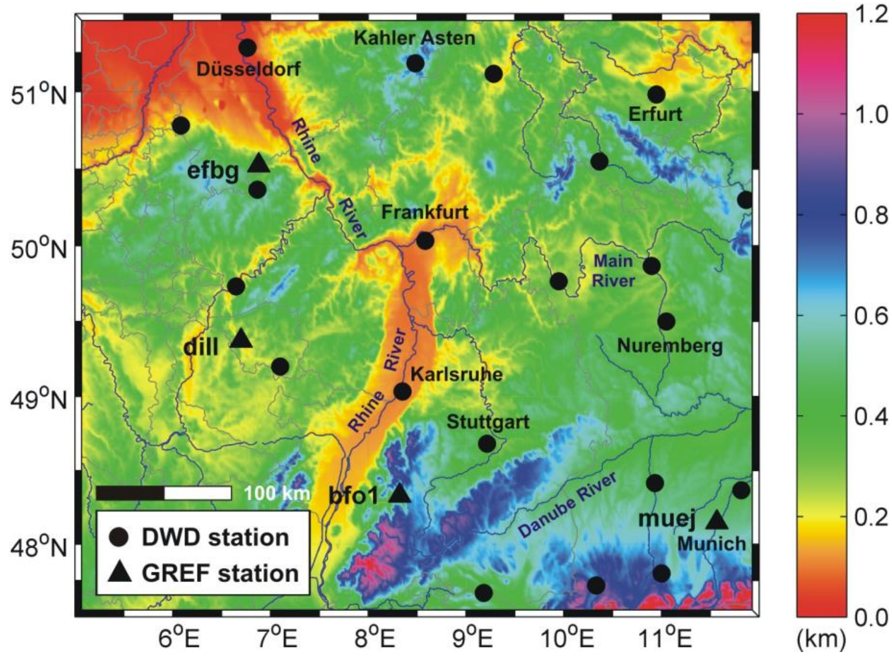

Figure 1: Selected DWD meteorological sites and GREF GNSS stations in the area of southwest Germany (digital elevation model: ETOPO1; Amante and Eakins, 2009).

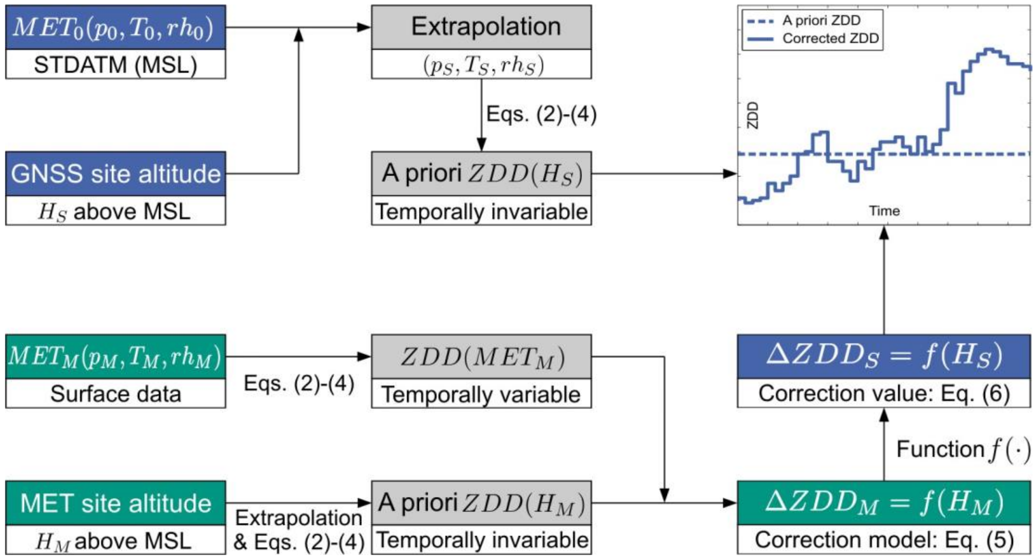

Figure 2: Schematic presentation of a height-dependent correction model for the GNSS a priori ZDD using regional surface meteorological data (STDATM: standard atmosphere, MSL: mean sea level, index $\boldsymbol{S}/\boldsymbol{M}$: GNSS/meteorological sites).

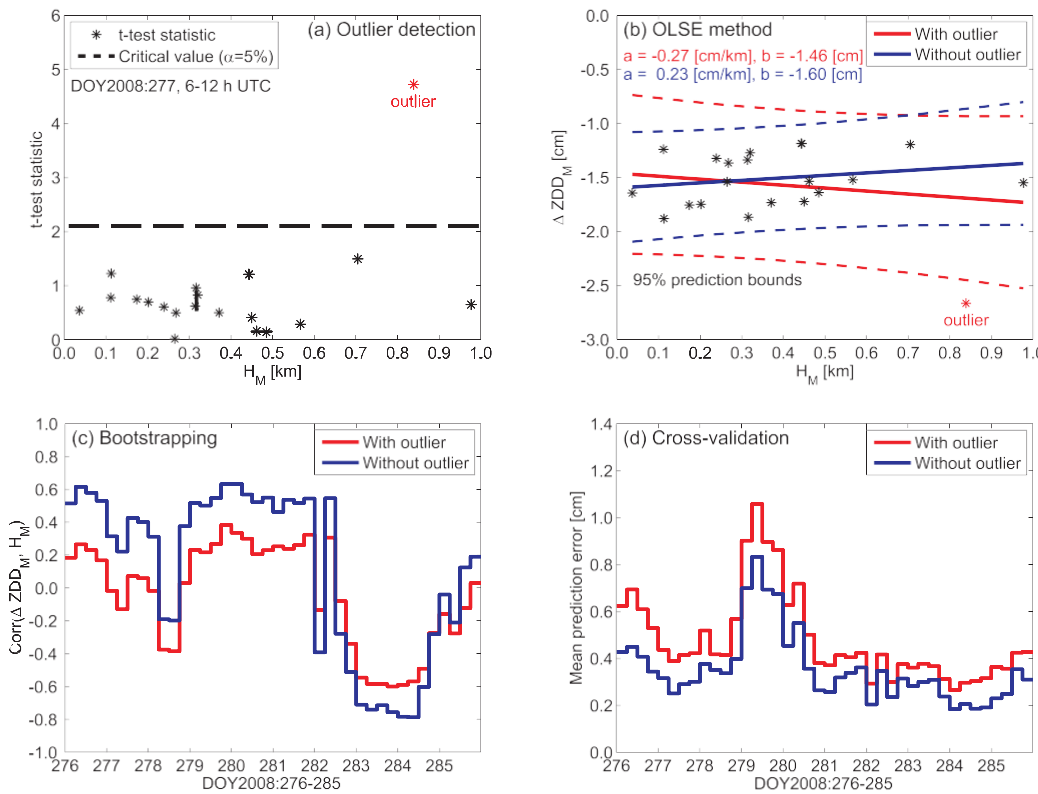

Figure 3: Example of outlier detection and its impact on linear regression using different methods (a) Outlier detection based on studentised residuals and Student's t-statistics (α = 5%), (b) Regression lines resulting from the ordinary least-squares estimation (OLSE), (c) Pearson's correlation coefficients from bootstrapping, (d) Mean prediction errors from the cross-validation method (see Eq. (12)).

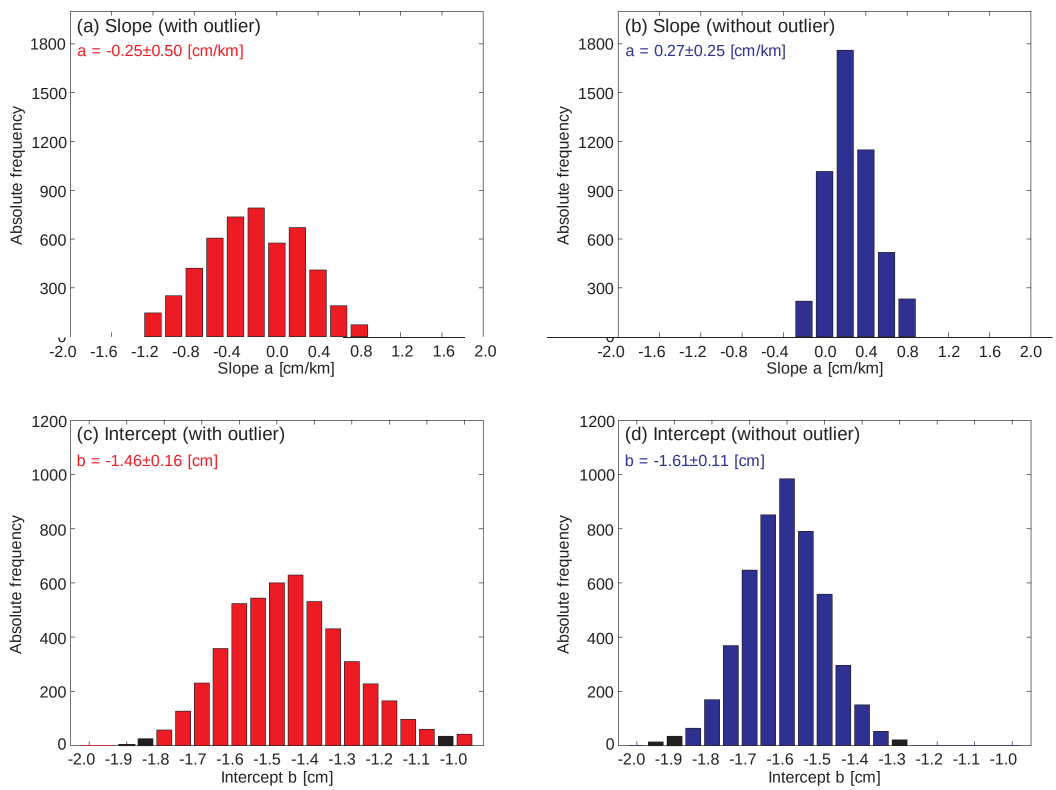

Figure 4: Histograms of the linear regression coefficients estimated by means of bootstrapping with 5000 samples (DOY2008:277, 6 – 12 h UTC, cf. Fig. 3b).

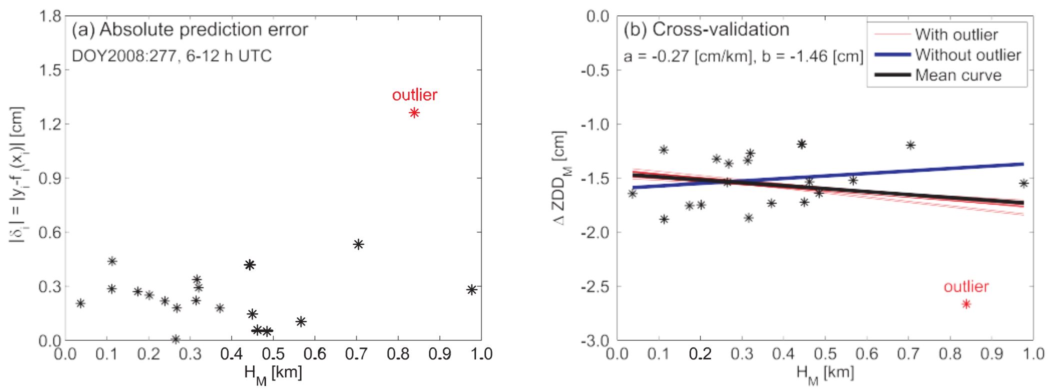

Figure 5: Example of linear regression using the leave-one-out cross-validation method (a) Outlier detection based on absolute prediction errors $|b_i|$ (see Eq. (11), cf. Fig. 3a), (b) Results of the linear regression (cf. Fig. 3b).

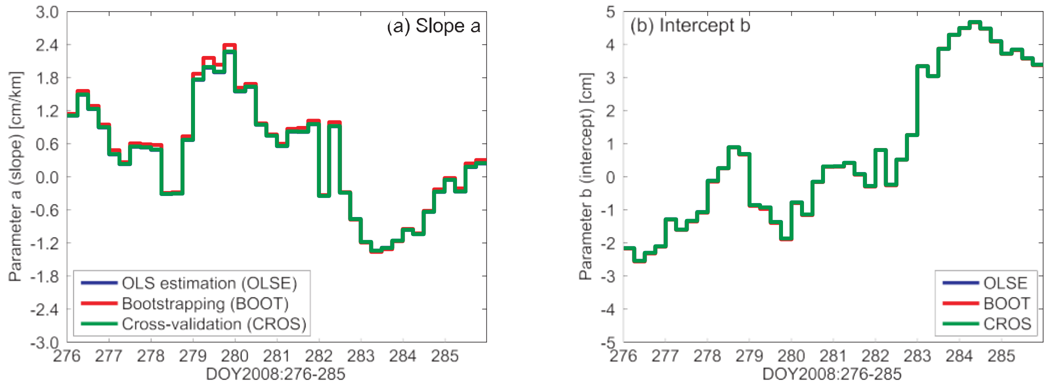

Figure 6: Comparison of the linear regression coefficients a (slope) and b (intercept) obtained by applying different parameter estimation methods after outlier removal. The mean results from bootstrapping and cross-validation are used for this comparison.

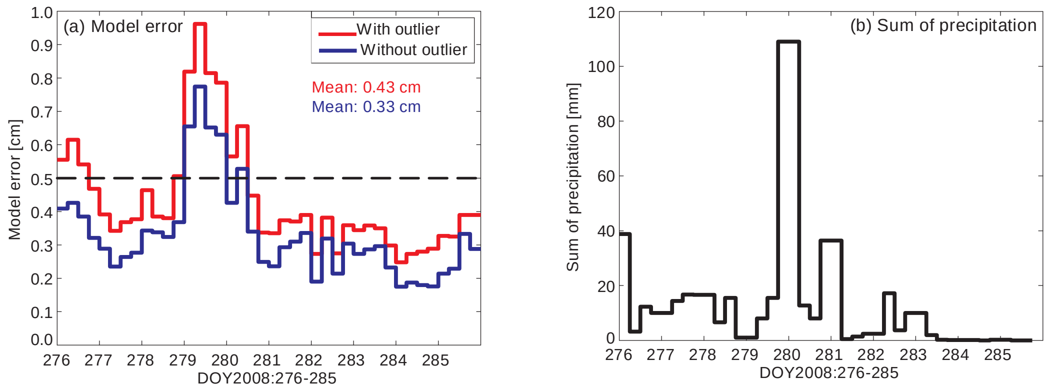

Figure 7: Impact of precipitation on the model error defined as the standard deviation of the least-squares residuals $\boldsymbol{v}_i$ (see Eq. (8)).

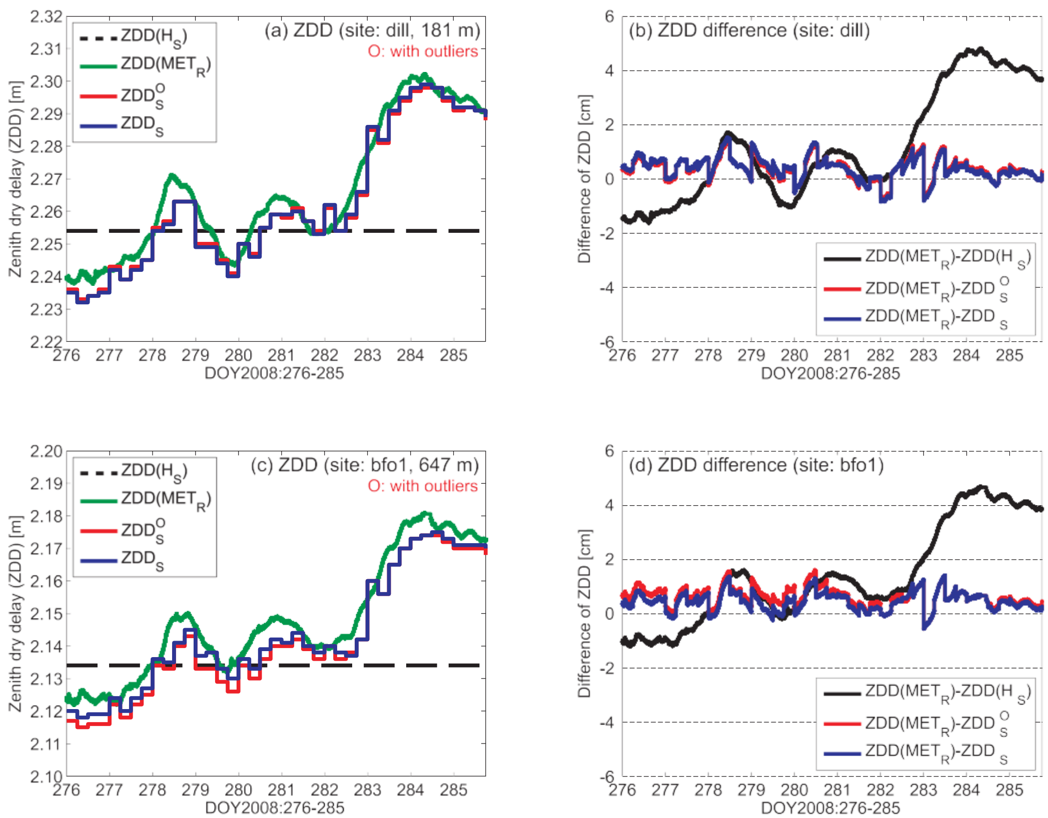

Figure 8: Model validation using representative GNSS stations with near-site meteorological measurements (a) and (c) A priori $ZDD(H_S)$, reference $ZDD(MET_R)$, and corrected ZDD_S values, (b) and (d) Biases from the reference values (see Eq. (7) for ZDD_S).

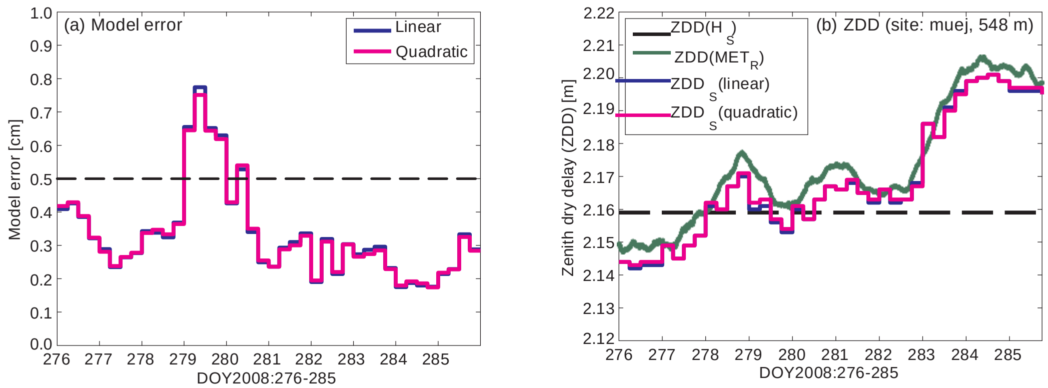

Figure 9: Comparison of the ZDD correction model using linear and quadratic regression (see Eqs. (5) and (14), without outliers, OLSE method) (a) Model error defined as the standard deviation of the least-squares residuals, (b) A priori $ZDD(H_S)$, reference $ZDD(MET_R)$, and corrected ZDD_S values.